Simultaneous Baseband and RF Optical Modulation Scheme for Feeding Wireless and Wireline Heterogeneous Access Networks

Alejandro Martinez, *Student Member, IEEE*, Valentin Polo, *Student Member, IEEE*, and Javier Marti, *Member, IEEE*

***Abstract*—In this paper, a novel modulation scheme that allows broad-band optical data transmission at both baseband and millimeter-wave RF carriers at twice the local-oscillator frequency is investigated. The dispersion-induced carrier suppression may be overcome by properly setting the optical transmitter parameters. Three different configurations for the modulation scheme are modeled and simulation and experimental results are provided. The key parameters of these configurations are optimized in order to achieve the best performance in broad-band heterogeneous millimeter-wave wireless and wireline access networks.**

***Index Terms*—Dispersion, fiber-wireless access networks, Gb/s networks, optical modulation, RF on fiber, wireline access networks.**

I. Introduction

NEXT-GENERATION broad-band wireless access networks are focusing intense research due to their moderate cost per user, bi-directionality, and ease of installation [1]. Coexistence of both wireline and wireless access networks within a metropolitan area network (MAN) is an important requirement for ensuring transparency in the node access. Future bandwidth requirements of access networks (in the Gb/s range) imposes the use of optical fiber for feeding several/many remote wireless base stations (BSs) from a central station (CS), especially for operation in the millimeter-wave frequency band [2], and wireline access nodes.

Regarding fiber-fed wireless BS techniques, several approaches can be found in the literature. The most desirable approach is that based on remote delivery of millimeter-wave signals from a central station (CS) to the BS antennas [3]. This scheme has many advantages as it allows for the centralized control of the generated signals and simplified BS configuration, reducing the overall cost of the network. However, the transmission of millimeter-wave signals through the optical fiber suffers from the impact of the fiber chromatic dispersion, which is known as the carrier suppression effect [4]. There are many techniques to mitigate this impairment [5]–[9]. Although optoelectronic devices performance has experienced a significant improvement [10], the electrooptical conversion response of such devices severely limits the overall performance of the system reducing the millimeter-wave fiber-wireless system power budget.

An alternative approach is to remote the local oscillator (LO) signal from CS to BS, in which the LO signal is extracted and used to up-convert the information signal electrically to the desired millimeter-wave frequency [11]. Some novel alternative schemes have been recently reported which achieve simultaneous transmission of baseband (BB) and LO signals [12], [13]. In [13], bi-directional operation was also demonstrated in for data speeds up to 622 Mb/s (downstream) and 155 Mb/s (upstream). In such schemes, a millimeter-wave electrical mixer is still required to upconvert the information signal to the millimeter-wave band, which impairs the cost and simplicity of the BS. In centralized architectures, the cost of the overall network will rely on simplified and moderate-cost BSs. From the authors' point of view, this is an advantage of the technique proposed in this paper, as simplified BSs are proposed with an increase of the cost of the equipment placed in the CS.

In this paper, we present three different configurations of a novel optical modulation scheme for simultaneous broad-band data transmission at BB and radio frequency (RF), which allow coexistence of optically fed wireline and wireless access network nodes within the same MAN. The proposed configurations are based on the use of a dual-electrode Mach–Zehnder modulator and have the following features: 1) simultaneous BB and RF modulation at twice the LO frequency of an optical carrier and 2) mitigation of the carrier suppression effect caused by the fiber chromatic dispersion in millimeter-wave frequency transmissions. The parameters of the optical modulation scheme can be optimized for achieving best performance depending on the node architecture [14]. In addition, it is also possible to implement simultaneous LO remoting under certain combination of the transmitter parameters.

The paper is organized as follows. In Section II, the theoretical model for the three configurations is presented and the optimum operating points are discussed. The theoretical model is validated by means of simulations using a commercial simulation package in Section III. In Section IV, a comparison of all the proposed configurations and the influence of system parameters on the performance of each configuration is carried out. In Section V, experimental results for one of the configurations is presented. Finally, conclusions are provided in Section VI.

Manuscript received January 5, 2001; revised May 30, 2001. This work was supported by the European Commission Project IST-2000-25390 and by the Spanish Research and Technology Commission (CICYT) Project TAP99-0443-C05-03.

The authors are with the Fiber-Radio Group, ITACA Research Institute, ETSI Telecomunicacion, Universidad Politecnica de Valencia, 46022 Valencia, Spain (e-mail: frg@upvnet.upv.es).

Publisher Item Identifier S 0018-9480(01)08695-1.

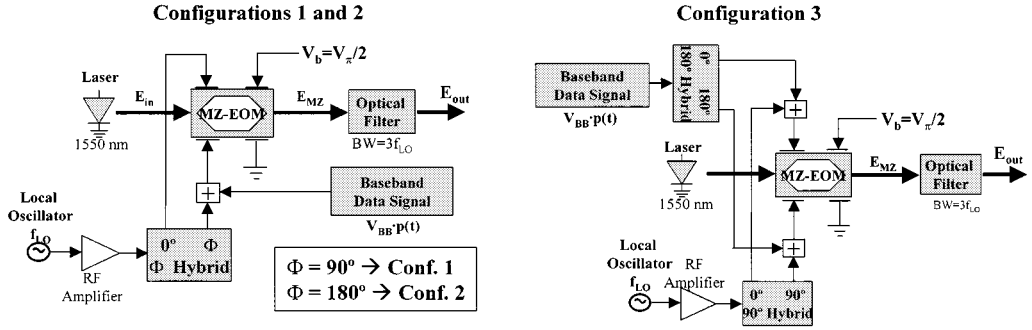

Fig. 1. Modulation schemes of the three configurations.

II. Theory and Model

A. Modulation Scheme

Fig. 1 depicts the three configurations of the proposed modulation scheme, named configurations 1, 2, and 3. They are based on the use of a dual-electrode Mach–Zehnder modulator (DE-MZM) biased at the quadrature point, which externally modulates a CW laser source. In all configurations, one of the DE-MZM RF ports is driven by a digital BB signal combined with an LO tone of frequency f_{LO}. The difference between the three configurations consists of the nature of the signal applied to the second RF port of the DE-MZM. In configuration 1, the second RF port is driven by a 90° phase-shifted LO tone obtained at the hybrid coupler output, whereas in configuration 2 a 180° hybrid coupler is used to generate that signal. In configuration 3, the second RF port is driven by the 90° phase-shifted LO signal combined with the inverted BB data signal. An optical filter is used to reject the undesired optical sidebands, as proposed in [13]. Extreme care must be taken in ensuring that the 90° or 180° phase and amplitude difference between both RF electrodes remains constant and equal to the required values. In other case, performance might be severely affected by the chirp-induced effects arising inherent to fiber-optic transmissions [6].

Theoretical expressions of the optical field at the filter output have been obtained, using a sinusoidal DE-MZM model. For configuration $i\,(i = 1, 2, 3)$, the optical field at the output of the filter (E^i_{out}) may be expressed as

$$\begin{aligned} E^1_{\mathrm{out}} = \frac{E_{\mathrm{in}}}{2}(&-J_0(\alpha)\cdot(1+p(t)\cdot\sin\gamma)\cdot\sin(\omega_0 t)+\cos\gamma \\ &\cdot J_0(\alpha)\cdot\cos(\omega_0 t)+-J_1(\alpha)\cdot(1+\cos\gamma) \\ &\cdot\cos(\omega_0-\omega_{\mathrm{LO}})t-J_1(\alpha)\cdot(1-\cos\gamma) \\ &\cdot\cos(\omega_0+\omega_{\mathrm{LO}})t+-p(t)\cdot\sin\gamma\cdot J_1(\alpha) \\ &\cdot[\sin(\omega_0+\omega_{\mathrm{LO}})t-\sin(\omega_0-\omega_{\mathrm{LO}})t]) \end{aligned} \tag{1a}$$

$$\begin{aligned} E^2_{\mathrm{out}} = \frac{E_{\mathrm{in}}}{2}(&-J_0(\alpha)\cdot(1+p(t)\cdot\sin\gamma)\cdot\sin(\omega_0 t)+\cos\gamma \\ &\cdot J_0(\alpha)\cdot\cos\,\omega_0 t+-J_1(\alpha)\cdot(1-\sin\gamma\cdot p(t)) \\ &\cdot(\cos(\omega_0-\omega_{\mathrm{LO}})t+\cos(\omega_0+\omega_{\mathrm{LO}})t)+J_1(\alpha) \\ &\cdot\cos\gamma\cdot(\sin(\omega_0+\omega_{\mathrm{LO}})t+\sin(\omega_0-\omega_{\mathrm{LO}})t)) \end{aligned} \tag{1b}$$

$$\begin{aligned} E^3_{\mathrm{out}} = \frac{E_{\mathrm{in}}}{2}&\cdot(\sqrt{2}\cdot J_0(\alpha)\cdot(\cos\gamma-p(t)\cdot\sin\gamma) \\ &\cdot\cos(\omega_0 t+\pi/4)+-2\cdot J_1(\alpha)\cdot\cos\gamma \\ &\cdot\cos(\omega_0-\omega_{\mathrm{LO}})t+2\cdot J_1(\alpha)\cdot p(t)\cdot\sin\gamma \\ &\cdot\sin(\omega_0+\omega_{\mathrm{LO}})t) \end{aligned} \tag{1c}$$

where E_{in} and ω_0 are the amplitude and the angular frequency of the input electric field, $p(t)$ represents the $[-1, +1]$ bipolar square NRZ data signal, and $J_0(.)$ and $J_1(.)$ stand for the zeroth- and first-order Bessel functions of the first kind, respectively, whose arguments are

$$\alpha = \frac{\pi\cdot V_{\mathrm{LO}}}{V_\pi} \tag{2a}$$

$$\gamma = \frac{\pi\cdot V_{\mathrm{BB}}}{V_\pi} \tag{2b}$$

where V_π is the half-wave voltage of the DE-MZM and V_{LO} and V_{BB} are the LO and BB data voltages, respectively. In order to obtain the theoretical optical field expressions using the DE-MZM sinusoidal model, a constant modulator electrodes transfer function over the data signal bandwidth, and therefore a constant V_π, has been assumed. It has been also considered that the digital signal is a random binary sequence composed by perfectly square NRZ bipolar pulses. The modulator insertion loss has not been considered in calculations as it has not electrical frequency dependence. From (1a) and (1b), it should be noticed that data appear both on the optical carrier (f_0) and on the two sidebands $(f_0 \pm f_{\mathrm{LO}})$. The only difference between both configurations is the amplitude of the sideband carriers: in configuration 1, the two sidebands have different levels depending on V_{BB}. Therefore, from (1a), when $V_{\mathrm{BB}} = 0(\cos\gamma = 1)$, no data signal drives the MZM and a f_{LO} tone is SSB modulated as the $f_0 + f_{\mathrm{LO}}$ sideband disappears [6]. On the other hand, when $V_{\mathrm{BB}} = V_\pi/2(\cos\gamma = 0)$, both sidebands have the same level. From (1b), it may be noticed that for configuration 2 both sidebands have the same level, which results in a f_{LO} carrier dispersion-induced fading after detection [4]. Finally, from (1c), it may be derived that in configuration 3 data are modulated onto the optical carrier and only one sideband will be generated, in this case the upper sideband at frequency $f_0 + f_{\mathrm{LO}}$, while only an unmodulated carrier appears as the lower sideband at frequency $f_0 - f_{\mathrm{LO}}$. As in configuration 1, this effect is due to the 90°-hybrid coupler that generates SSB modulation, but here in both data and the f_{LO} signal.

B. Fiber Transmission Theory

When the modulated optical signal is transmitted through an SSMF link, whose length and dispersion parameter are L (km) and D (ps/nm/km), respectively, it suffers a degradation due to the fiber chromatic dispersion that results in a power penalty of

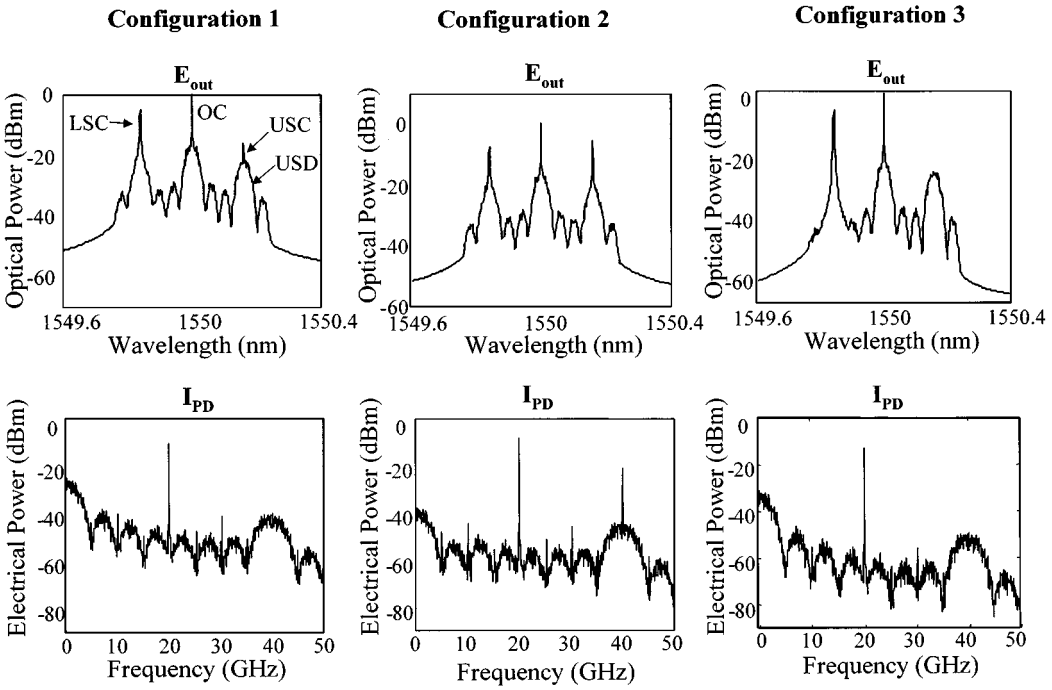

Fig. 2. Simulation results: ideal optical spectra at the filter output and photodetected current spectra after amplification for configuration 1 ($V_{\rm BB} = V_\pi/4 = 2.5\,V$), configuration 2 ($V_{\rm BB} = V_\pi/4 = 2.5$ V), and configuration 3 ($V_{\rm BB} = V_\pi/8 = 1.25$ V). Parameters: $L = 0$ km, $f_{\rm LO} = 20$ GHz, $R_b = 5$ Gb/s, $P_{\rm LO} = +20$ dBm. LSC: lower sideband carrier; OC: optical carrier; USC: upper sideband carrier; USD: upper sideband data.

the photodetected signal [4]. At the receiving end, three significant terms of the photocurrent for each configuration are obtained at BB and $2f_{\rm LO}$. These terms are

at BB

$$I^1_{\rm BB} \propto 2\cdot J_0^2(\alpha)\cdot(1+p(t)\cdot\sin\gamma)+4\cdot J_1^2(\alpha) \tag{3a}$$

$$I^2_{BB} \propto 2\cdot J_0^2(\alpha)+4\cdot J_1^2(\alpha)+2\sin\gamma\cdot p(t)\cdot(J_0^2(\alpha)-2\cdot J_1^2(\alpha)) \tag{3b}$$

$$I^3_{\rm BB} \propto 2\cdot J_0^2(\alpha)+4\cdot J_1^2(\alpha)-2\cdot J_0^2(\alpha)\cdot\sin\gamma\cdot\cos\gamma\cdot p(t) \tag{3c}$$

and, at $2f_{\rm LO}$

$$I^1_{2f_{\rm LO}} \propto 4\cdot J_1^2(\alpha)\cdot\sin\gamma\cdot p(t)\cdot\sin(2\omega_{\rm LO}t) \tag{4a}$$

$$I^2_{2f_{\rm LO}} \propto 4\cdot J_1^2(\alpha)\cdot(1-\sin\gamma\cdot p(t))\cdot\cos(2\omega_{\rm LO}t) \tag{4b}$$

$$I^3_{2f_{\rm LO}} \propto 8\cdot J_1^2(\alpha)\cdot\sin\gamma\cdot\cos\gamma\cdot p(t)\cdot\sin(2\omega_{\rm LO}t) \tag{4c}$$

where $\beta = \pi\cdot L\cdot D\cdot\lambda^2/c$, λ is the laser wavelength, c is the vacuum velocity of light, and $I^i_{\rm BB}$ and $I^i_{2f_{\rm LO}}$ stand for the photodetected current for each configuration ($i = 1, 2, 3$). The LO power ($P_{\rm LO}$) influences the detected current through the α parameter in the Bessel functions. From (3a) to (3c) and (4a) to (4c), it may be observed that if data recovering simultaneously at both BB and RF ($2f_{\rm LO}$) is desired there would be a tradeoff in selecting the optimum LO power. The latter would be such a case of a node of the MAN is fed as BB for a wireline access network and another node is fed as RF for a wireless access network.

From (3a) to (3c), it should be noticed that the BB data can be recovered at the receiver for any configuration. Likewise, it can be seen in (4a)–(4c) that the data signal $p(t)$ is modulated onto a $2f_{\rm LO}$ carrier that does not suffer the carrier suppression effect, as no dependence of $I^i_{2f_{\rm LO}}$ on the β parameter exists. In configurations 1 and 2, four $2f_{\rm LO}$ beats are generated in the photodetection process, as can be deduced from (1a) and : carrier–carrier, data–data, and two data–carrier beats. Both carrier–data beats have the same phase and produce terms described in (4a) and (4b). If we consider that the BB data signal pulses are polar $[-1, +1]$ and perfectly squared, the data-data beat generates a $2f_{\rm LO}$ single tone term. If the pulses are not square (e.g., super Gaussian, raised-cosine, etc.), the data-data beat originates a $p^2(t)$ distortion term onto the $2f_{\rm LO}$ frequency. It has been observed that this undesired term is in-quadrature with the desired $2f_{\rm LO}$ data component, when assuming not perfectly square pulses. It may also be noticed that in configuration 2, a $2f_{\rm LO}$ carrier appears with the modulated data, whereas in the other configurations only modulated data are observed. The ideal simulated spectra at the filter output is depicted in Fig. 2, showing for each configuration the optical components corresponding to (1), that generate the electrical terms described by (3) and (4).

The optimum $V_{\rm BB}$ for maximum modulated data recovering is $V_{\rm BB} = V_\pi/2$ in configurations 1 and 2 (since $\sin\gamma = 1$), while it is $V_{\rm BB} = V_\pi/4$ in configuration 3 (since $\sin 2\gamma = 2\sin\gamma\cos\gamma = 1$). This is due to the fact that in configuration 3 BB data drive both RF ports of the DE-MZM and half of the BB signal voltage level is needed for achieving the same modulation depth. On the other hand, by employing configurations 1 and 3 with the 90° hybrid coupler, a dispersion-tolerant $f_{\rm LO}$ tone can be also obtained under certain data amplitude conditions. This LO remoting feature may be interesting to implement the uplink receiving part in the BS. A detailed discussion on this LO

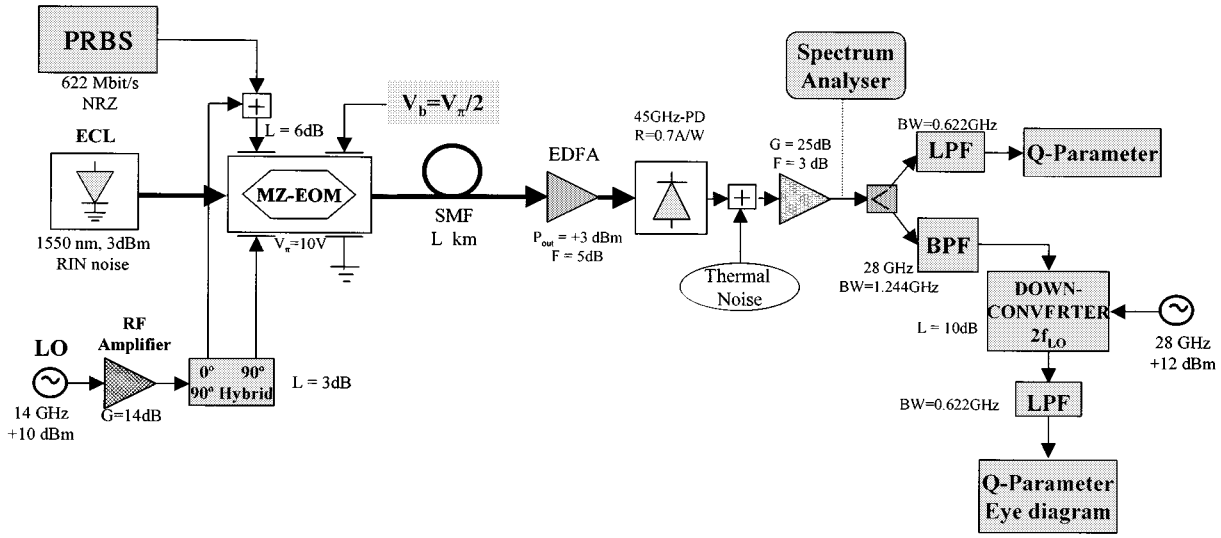

Fig. 3. Q-factor measure simulation scheme for configuration 1.

remoting feature is beyond the scope of this paper and will be presented elsewhere.

III. Simulation Results

In order to validate the theoretical model described above using a realistic optical data transmission framework, the three configurations of the modulation scheme have been simulated on a commercial package (Optsim). Fig. 2 shows the optical spectra at the filter output and the preamplifier photodetected current spectra for the three configurations, for a 0-km fiber span. The LO frequency and power are $f_{\rm LO} = 20$ GHz and $P_{\rm LO} = +20$ dBm, respectively. The NRZ BB data is generated by a $2^{15} - 1$ PRBS generator which rate is $R_b = 5$ Gb/s, with amplitude $V_{\rm BB} = V_\pi/4$ for configurations 1 and 2, and $V_{\rm BB} = V\pi/8$ for configuration 3. These amplitudes have been chosen to be half the optimum value for all three schemes, therefore data at both BB and $2f_{\rm LO}$ are modulated and also the $f_{\rm LO}$ tone might be recovered at the receiving end, if required for bi-directional operation of the BS. The half-wave voltage (V_π) of DE-MZM is assumed to be 10 V and therefore is quadrature biased for $V_b = 5$ V. For the sake of comparison with the theoretical model, no frequency dependence of V_π has been considered. The optical filter has a $3f_{\rm LO} = 60$-GHz bandwidth that rejects second-order and higher order harmonics. The receiver consists of a 45-GHz PD, a 25-dB gain broad-band preamplifier, and an electrical spectrum analyzer. It may be observed that the simulation results for the three configurations depicted in Fig. 2 agree very well with the discussion on the obtained theoretical expressions for $E_{\rm out}$ and $I_{\rm PD}$ (photodetected current) given in Section II.

In order to verify the dispersion effects on the transmitted signal RF power as a function of the fiber length, simulations have been carried out. In a conventional double sideband (DSB) amplitude modulation RF optical transmission, power fading appears in the detected signal due to chromatic dispersion [4]. The RF photodetected current depends on the term $\cos(\beta f_{\rm RF}^2)$, where $f_{\rm RF}$ is the modulation frequency. Simulations have confirmed that the transmitted $2f_{\rm LO}$ carrier does not suffer from the carrier suppression effect when transmitted through a standard SSMF, as it was predicted by the theoretical results for the three proposed modulation schemes.

IV. Performance Comparison

In this section, the performance of the three configurations of the proposed modulation scheme are compared and optimized depending on the required functionality. By comparing the three configurations in terms of BB detected current, it can be deduced from (3) that 90° hybrid-based configurations are more efficient than configuration 2. This is due to the fact that in the latter the data modulated onto the two optical sidebands are in phase opposition with the data modulated onto the optical carrier. Moreover, it should be noticed from (3b) that the detected BB data vanish when $J_0^2(\alpha) = 2 \cdot J_1^2(\alpha)$, which occurs if $P_{\rm LO} = +21.345$ dBm $(Z_0 = 50\,\Omega)$. This result has been validated by means of simulation. From (3), if we compare the expressions for configurations 1 and 3, it is noticed that $I_{\rm BB}^1/I_{\rm BB}^3 = -2\,\cos\gamma$, so $V_{\rm BB}$ is the parameter that determines which configuration has the better performance. By comparing (4a) and (4b), it can be concluded that the recovered $2f_{\rm LO}$ modulated data in both configurations 1 and 2 have the same amplitude although both signals are in phase-opposition. On the other hand, the relationship between the detected current at $2f_{\rm LO}$ in configurations 1 and 3 is $I_{2f_{\rm LO}}^1/I_{2f_{\rm LO}}^3 = 2\,\cos\gamma$, so better performance will also depend on $V_{\rm BB}$.

The previous considerations have been confirmed by means of simulation. Realistic system conditions have been considered including passive devices losses (hybrid coupler, combiner, mixer) and noise sources: relative intensity noise (RIN) from the laser source, amplified spontaneous emission (ASE) noise generated by the erbium-doped fiber amplifier (EDFA), shot noise in the PIN-PD, and thermal noise after photodetection (18.2 pA/$\sqrt{\rm Hz}$). The simulation scheme used for configuration 1 is depicted in Fig. 3. A distributed-feedback (DFB) Bragg laser is externally modulated using a DE-MZM ($V_\pi = 10$ V, ER $= 25$ dB, BW $= 35$ GHz, $L_{\rm ins} = 3$ dB) biased at quadrature. The laser wavelength is 1550 nm with $+3$ dBm of power

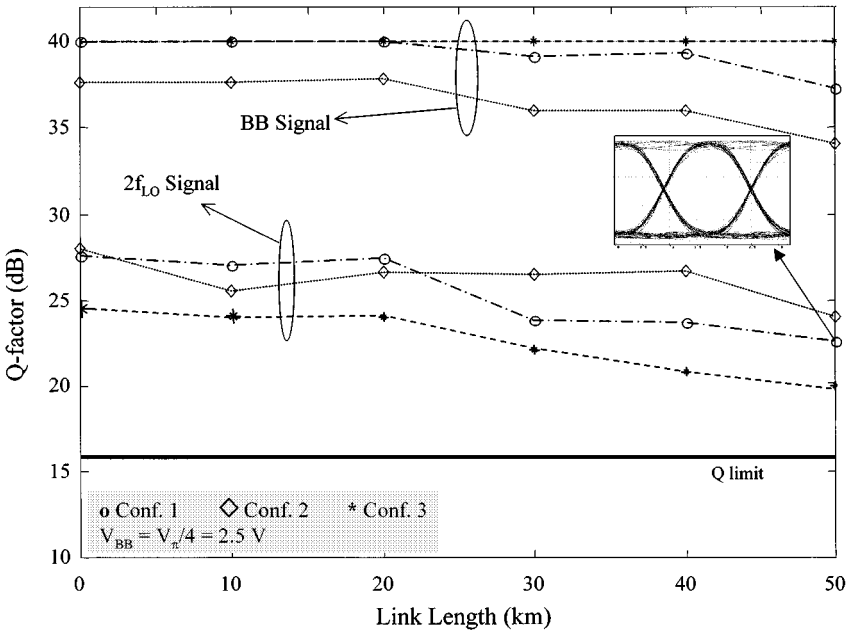

Fig. 4. Simulation results: BB and RF signal Q-factor versus link length.

and $\mathrm{RIN} = -148$ dB/Hz. A 14-GHz LO tone is amplified up to $+24$ dBm using a millimeter-wave amplifier and is injected into a 90° hybrid-coupler with 3-dB insertion loss. As shown in Fig. 1, for configuration 2, a 180° hybrid-coupler is used. A 622-Mb/s PRBS NRZ polar data signal is combined with the LO amplified tone using a 6-dB-loss electrical combiner. In configuration 3, an additional combiner is needed to inject the data signal in both MZM RF ports, as shown in Fig. 1. A SSMF coil with $D = 15.62$ ps/nm/km and variable length links the transmitter and receiver. A fixed output power EDFA is used to compensate for the fiber loss delivering a $+3$ dBm power optical signal at the PIN-PD input. The PD has a 0.7-A/W responsivity and a 45-GHz bandwidth. A thermal noise source is modeled and added to the signal. A 25-dB-gain broad-band amplifier with $F = 3$ dB pumps the signal and a power divider is used to split the signal for BB and RF analyzing. In the BB path, a low-pass Bessel filter rejects the undesired RF components. A bandpass Bessel filter centered at 28 GHz is used in the RF path to recover the $2f_{\mathrm{LO}}$ component, followed by a mixer with 10-dB conversion loss and $F = 3$ dB. A 28-GHz variable phase LO signal with $+12$-dBm power is injected to the mixer. After downconversion, the desired signal is filtered using a low-pass Bessel filter. The Q-factor of both recovered signals is estimated using a digital communications analyzer.

Fig. 4 shows the obtained Q-factor for both BB and RF received signals when the fiber link length varies from 0 to 50 km. The maximum Q-factor value that can be calculated by the simulator is 40 dB. As expected from theoretical results, the BB Q-factor for configuration 2 is worse than for the others (3 dB lower than configuration 1), although the data signal can be perfectly recovered with $Q > 34$ dB for the three modulations schemes, with configuration 3 having the best results. The downconverted $2f_{\mathrm{LO}}$ signal Q-factor values when $V_{\mathrm{BB}} = V_{\pi}/4$ are similar for the three schemes and $Q = 19.5$ dB in the worst case, higher than the Q limit (15.66 dB for $\mathrm{BER} = 10^{-9}$).

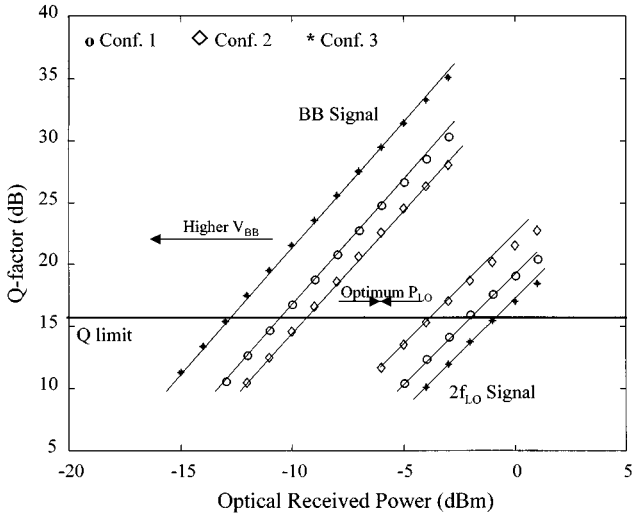

Fig. 5. Simulated Q-factor as a function of the received optical power for both baseband and RF received data.

Configuration 3 shows lower performance due to the additional loss introduced by the 180° hybrid coupler used to invert the data stream. No power fading due to chromatic dispersion is observed, which confirms that the technique is dispersion-tolerant. Fig. 4 inset shows the eye diagram obtained using configuraiton 1 for $L = 50$ km.

Fig. 5 depicts the Q-factor for both BB and RF recovered data as a function of the optical power that impinges on the PD. The receiver sensitivity for RF data may be improved by increasing the LO power, V_{BB}, or both. From Fig. 5, it can also be noticed that the behavior of each configuration in BB an RF is opposed: the best configuration for BB (configuration 3) is the worst for RF, and conversely. There is a tradeoff between the BB and the RF behavior that depends on the LO power. If an adequate LO power is chosen, the BB and RF behavior can become identical

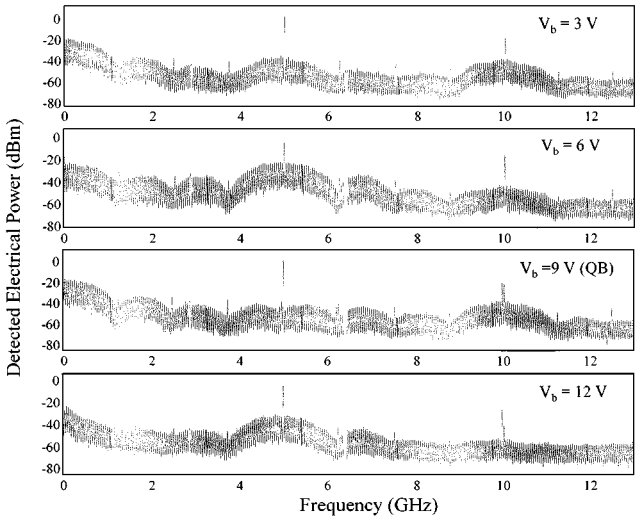

Fig. 6. Electrical spectra at the photoreceiver output for different DE-MZM bias voltages.

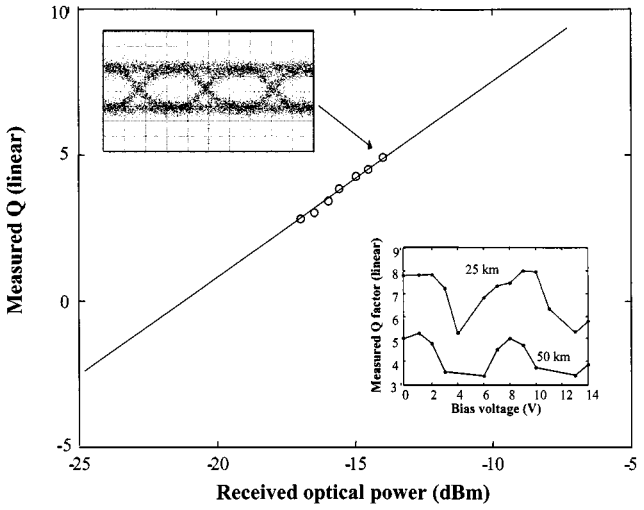

Fig. 7. Q-factor for BB 622-Mb/s transmission as a function of the received optical power (DE-MZM in quadrature). The inset shows the measured Q-factor for BB 622-Mb/s transmission as a function of the DE-MZM bias voltage for 25- and 50-km fiber spans.

and good performance can be achieved simultaneously at BB and RF.

The technique robustness against the bias voltage variations for both BB and RF data signals has also been estimated. The simulations show that a variation greater than 1 V around the optimum bias point only varies the Q-factor around a half a decibel.

V. Experimental Results

Experimental measurements using configuration 1 have been carried out. A detailed description of the experimental setup can be found in [14]. In order to evaluate the influence of the DE-MZM bias voltage, the electrical spectrum at the PD output for a 1.25-Gb/s PRBS signal and a $f_{\rm LO}$ of 5 GHz when transmitting over a 50-km fiber span was obtained, as shown in Fig. 6. In this figure, it can be noticed that depending on the DE-MZM bias voltage, the data spectrum moves from $f_{\rm LO}$ to BB and $2f_{\rm LO}$. These results fully agree with the theoretical formulas and simulations.

The performance of the received signal at BB and at $2f_{\rm LO}$ was also measured. Fig. 7 shows the measured Q-factor for a 622-Mb/s BB signal as a function of the received optical power, and the inset shows the same parameter as a function of the DE-MZM bias voltage for 25- and 50-km fiber-optic spans. A Q-factor of six $(\mathrm{BER} = 10^{-9})$ may be achieved for a received optical power around -12 dBm. In the inset of Fig. 7, it may be observed that good performance is obtained for the BB broad-band data when the DE-MZM is biased in quadrature ($V_b = 1$ V or $V_b = 8.5$ V) and that the system performance sensitivity to the DE-MZM bias voltage is moderate.

Finally, Fig. 8 shows the measured Q-factor for a 52-Mb/s data signal upconverted to $2f_{\rm LO}$ (@10.24 GHz) as a function of the bias voltage. Those data rates and frequencies were selected due to laboratory equipment limitations. Fig. 8 shows that a $Q \sim 8\,(\mathrm{BER} < 10^{-11})$ is achieved at the quadrature points after downconversion of the $2f_{\rm LO}$ signal. It should be noticed that the quadrature points for BB and $2f_{\rm LO}$ are different due to the frequency variation of the DE-MZM V_π parameter.

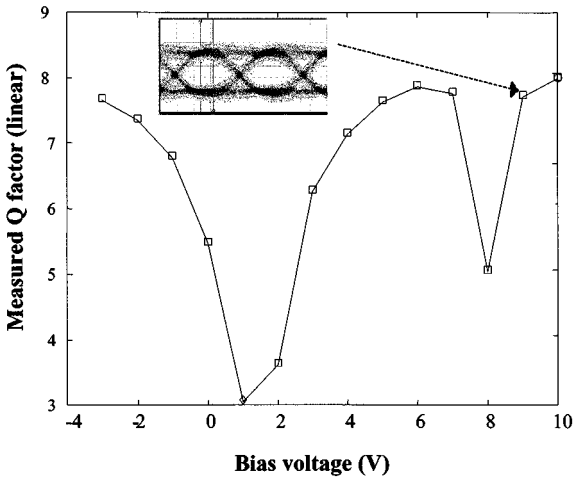

Fig. 8. Q-factor against the DE-MZM bias voltage for a 52-Mb/s transmission over 50-km fiber spans at $2f_{\rm LO}$ of 10.24 GHz.

We expect to obtain experimental results for configurations 2 and 3 soon. These results will allow us to make a comparison among the three configurations and to establish which configuration present the best global performance for dual BB and RF data on fiber links.

VI. Conclusion

A novel technique for simultaneous BB and dispersion-tolerant RF data signal transmission has been investigated. A dual-electrode Mach–Zehnder modulator biased at the quadrature point is the key device. Three different configurations of this technique have been modeled and simulations results have been achieved that are in good agreement with the obtained theoretical expressions. A comparison between the three configurations has been carried out through simulations. The robustness of the transmission technique against bias points variations has also been proved. Experimental results have been obtained for configuration 1 which confirm the theoretical expressions and

simulations. This modulation technique may be very useful in hybrid fiber-wireless access and wireline networks for up to several Gb/s data rates.

REFERENCES

[1] H. Loktu, P. Linna, E. Bigan, T. Kuitunen, A. Kelleher, and M. Matescu, "Status and future evolution of broadband radio access," in *Proc. NOC '98*, vol. I, 1998, pp. 222–229.

[2] R. Heidemann and G. Veith, "MM-wave photonics technologies for Gbit/s-wireless-local-loop," in *Proc. OECC'98*, Chiba, Japan, 1998, pp. 310–311.

[3] J. J. O'Reilly and P. M. Lane, "Remote delivery of video services employing using mm-waves and optics," *J. Lightwave Technol.*, vol. 12, pp. 369–375, Feb. 1994.

[4] H. Schmuck, "Comparison of optical millimeter-wave system concepts with regard to chromatic dispersion," *Electron. Lett.*, vol. 31, no. 21, pp. 1848–1849, 1995.

[5] J. Marti, J. M. Fuster, and R.I. Laming, "Experimental reduction of chromatic dispersion effects in lightwave microwave/millimeter-wave transmissions employing tapered linearly chirped fiber gratings," *Electron. Lett.*, vol. 33, pp. 1170–1171, 1997.

[6] G. H. Smith, D. Novak, and Z. Ahmed, "Overcoming chromatic dispersion effects in fiber-wireless systems incorporating external modulation," *IEEE Trans. Microwave Theory Tech.*, vol. 45, pp. 1410–1415, Aug., 1997.

[7] J. J. O'Reilly, P. M. Lane, R. Heidemann, and R. Hoffstetter, "Optical generation of very narrow linewidth millimeter-wave signals," *Electron. Lett.*, vol. 25, no. 3, pp. 2309–2311, 1992.

[8] R. Montgomery and R. Desalvo, "A novel technique for double sideband suppressed carrier modulation of optical fields," *IEEE Photon. Technol. Lett.*, vol. 7, pp. 434–436, Apr. 1995.

[9] G. H. Smith, D. Novak, C. Lim, and K. Wu, "Full-duplex broadband millimeter-wave optical transport system for fiber-wireless access," *Electron. Lett.*, vol. 33, no. 13, pp. 1159–1160, 1997.

[10] D. Decoster, "Microwave optoelectronic systems," in *Proc. EuMC'98*, vol. 1, 1998, pp. 485–496.

[11] D. J. Blumenthal, J. Laskar, R. Gaudino, S. Han, M. D. Schell, and M. D. Vaughn, "Fiber-optic links supporting baseband data and subcarrier multiplexed control channels and the impact of MMIC photonic/microwave interfaces," *IEEE Trans. Microwave Theory Tech.*, vol. 45, pp. 1443–1452, Aug. 1997.

[12] G. H. Smith and D. Novak, "Broadband millimeter-wave fiber-radio network incorporating remote up/downconversion," in *Proc. IEEE MTT-S Int. Microwave Symp. Dig.*, Baltimore, MD, 1998, pp. 1509–1512.

[13] C. Lim, A. Nimarthalas, D. Novak, R. Waterhouse, and G. Yoffe, "Millimeter-wave broad-band fiber-wireless system incorporating baseband data transmission over fiber and remote LO delivery," *J. Lightwave Technol.*, vol. 18, pp. 1355–1363, Oct. 2000.

[14] V. Polo, A. Martinez, J. Marti, F. Ramos, A. Griol, and R. Llorente, "Simultaneous baseband and RF modulation scheme in Gbit/s millimeter-wave wireless-fiber networks," in *Proc. MWP'00*, Oxford, U.K., paper WE2-5, pp. 168–171.

Alejandro Martinez (S'99) received the Ingeniero de Telecomunicacion degree from the Universidad Politecnica de Valencia, Valencia, Spain, in 2000, and is currently working toward the Ph.D. degree at the Universidad Politecnica de Valencia.

He is a member of the Fiber-Radio Group, Universidad Politecnica de Valencia. His research interests include applications of microwave and millimeter-wave radio over fiber systems, dispersion compensation, and optical integrated systems.

Valentin Polo (S'93) received the Ingeniero Superior de Telecomunicacion degree from the Universidad Politecnica de Valencia, Valencia, Spain, in 1997, and is currently working toward the Ph.D. degree at the Universidad Politecnica de Valencia.

He is a member of the Fiber-Radio Group, Universidad Politecnica de Valencia. His research interests include fiber-radio systems and applications, microwave and millimeter-wave photonics, optical beamforming, dispersion compensation, and broad-band access systems and technologies, including WLL, LMDS, DWDM-SCM, FTTx, HFC, and PON. He has co-authored over 30 papers in international journals and conferences. He has acted as reviewer for several international publications.

Javier Marti (S'89–M'92) received the Ingeniero de Telecomunicacion degree from the Universidad Politecnica de Catalunya, Catalunya, Spain, in 1991, and the Doctor Ingeniero de Telecomunicacion degree (Ph.D.) from the Universidad Politecnica de Valencia, Valencia, Spain, in 1994.

During 1989 and 1990, he was an Assistant Lecturer at the Escuela Universitaria de Vilanova, Barcelona, Spain. From 1991 to 2000, he was a Lecturer and Associate Professor at the Telecommunication Engineering Faculty, Universidad Politecnica de Valencia, where is currently Professor and leads the Radio over Fiber Group. He has authored or co-authored over 90 papers in refereed international technical journals and over 40 papers in international conferences in the fields of fiber-radio and microwave/millimeter-wave photonics, WDM and SCM optical networks systems, optical processing of microwave signals, dispersion, and fiber nonlinearities compensation employing fiber gratings and other techniques.

Prof. Marti is member of the Technical Program Committee of the ECOC and several other international workshops and conferences.